ORIGINAL ARTICLE

Mitochondrial RNA processing defect caused by a *SUPV3L1* mutation in two siblings with a novel neurodegenerative syndrome

Selma L. van Esveld[1] | Richard J. Rodenburg[2] | Fathiya Al-Murshedi[3] | Eiman Al-Ajmi[4] | Sana Al-Zuhaibi[5] | Martijn A. Huynen[1] | Johannes N. Spelbrink[2] ![ORCID]

[1]Radboud Center for Mitochondrial Medicine & Center for Molecular and Biomolecular Informatics, Radboud Institute for Molecular Life Sciences, Nijmegen, The Netherlands

[2]Radboud Center for Mitochondrial Medicine, Department of Paediatrics, Radboudumc, Nijmegen, The Netherlands

[3]Genetic and Developmental Medicine Clinic, Sultan Qaboos University Hospital, Muscat, Oman

[4]Department of Radiology and Molecular Imaging, Sultan Qaboos University Hospital, Muscat, Oman

[5]Department of Ophthalmology, Sultan Qaboos University Hospital, Muscat, Oman

Correspondence
Martijn A. Huynen, Radboud Center for Mitochondrial Medicine & Center for Molecular and Biomolecular Informatics, Radboud Institute for Molecular Life Sciences, Nijmegen, The Netherlands.
Email: martijn.huijnen@radboudumc.nl

Johannes N. Spelbrink, Radboud Center for Mitochondrial Medicine, Department of Paediatrics, Radboudumc, Geert Grooteplein 10, Nijmegen 6525GA, The Netherlands.
Email: hans.spelbrink@radboudumc.nl

Abstract

SUPV3L1 encodes a helicase that is mainly localized in the mitochondria. It has been shown in vitro to possess both double-stranded RNA and DNA unwinding activity that is ATP-dependent. Here we report the first two patients for this gene who presented with a homozygous preliminary stop codon resulting in a C-terminal truncation of the *SUPV3L1 protein*. They presented with a characteristic phenotype of neurodegenerative nature with progressive spastic paraparesis, growth restriction, hypopigmentation, and predisposition to autoimmune disease. Ophthalmological examination showed severe photophobia with corneal erosions, optic atrophy, and pigmentary retinopathy, while neuroimaging showed atrophy of the optic chiasm and the pons with calcification of putamina, with intermittent and mild elevation of lactate. We show that the amino acids that are eliminated by the preliminary stop codon are highly conserved and are predicted to form an amphipathic helix. To investigate if the mutation causes mitochondrial dysfunction, we examined fibroblasts of the proband. We observed very low expression of the truncated protein, a reduction in the mature *ND6* mRNA species as well as the accumulation of double-stranded RNA. Lentiviral complementation with the full-length *SUPV3L1* cDNA partly restored the observed RNA phenotypes, supporting that the *SUPV3L1* mutation in these patients is pathogenic and the cause of the disease.

KEYWORDS
degradosome, mitochondrial disease, mitochondrial RNA processing, mtDNA, neurodegenerative syndrome, *SUPV3L1*

1 | INTRODUCTION

Human mitochondrial disorders can be caused by a broad spectrum of mutations in either mitochondrial DNA (mtDNA) or nuclear DNA. Although mtDNA only contains a small number of genes (13 protein-coding, 22 tRNA, and 2 rRNA genes), its proper maintenance and gene expression is essential for the oxidative phosphorylation system. mtDNA is transcribed into two long polycistronic transcripts that require further processing and modifications to yield the functional pool of RNAs.[1-3] Proper mitochondrial RNA homeostasis in addition requires a machinery for the degradation of noncoding transcripts and aberrant RNA species, the mitochondrial RNA degradosome (mtEXO). It was shown to participate in processing of mitochondrial mRNA,[4,5] *16S* rRNA,[6] aberrant RNA species, and noncoding RNA (ncRNA),[7] including the 3′-end of *ND6*,[8] whose open reading frame, unlike most other mitochondrial pre-mRNAs, is not directly flanked by a tRNA. Noncoding RNAs are mainly derived from the light-strand templated polycistronic transcript that in vertebrates is G-rich due to the GC-skew of the mitochondrial genome. G-rich transcripts are prone to form G-quadruplex structures that in cytosolic RNA metabolism have been shown to interfere, among others, with pre-mRNA splicing, polyadenylation, and translation.[9] Pietras et al recently showed that mtEXO degradation of G-rich RNA is facilitated by the protein G-rich sequence factor 1 (GRSF1) that is thought to melt G-quadruplex structures.[10]

In humans, mtEXO consists of a polyribonucleotide nucleotidyltransferase 1 (PNPT1 or PNPase) and an ATP-dependent RNA helicase (SUPV3L1 or SUV3).[4] The first component is not conserved between yeast and mammals, but SUPV3L1 is ubiquitous in eukaryotes and has an evolutionarily conserved function.[11] SUPV3L1 is a helicase that depends on ATP hydrolysis[12,13] to move along the substrate in a 3′ to 5′ direction.[14,15] It requires a 3′ single-stranded overhang and is capable of unwinding RNA:DNA hybrids, dsRNA, and double-stranded DNA (dsDNA).[12,13] The protein was found to be located in the mitochondrial matrix[13] as well as the nucleus.[16]

Loss of mtEXO activity leads to the accumulation of double-stranded RNA (dsRNA)[17] probably due to improper processing of ncRNA and, in addition, results in the accumulation of DNA:RNA hybrids in mitochondria.[17] This suggested that mtEXO is important in counteracting deleterious R-loops, which form by persistent DNA:RNA hybrid formation that displaces the other DNA strand in dsDNA. Persistent R-loops could result in replication-transcription conflicts and genome instability[17] and could be detrimental to the cell.

In this article, we report for the first time two patients with a C-terminal homozygous nonsense mutation in the *SUPV3L1* gene. We show that the C-terminal protein region, which is missing due to the preliminary stop-codon, is well-conserved. In line with this, our results showed a mitochondrial light-strand RNA processing defect in patient cells that was partly restored after the introduction of the full-length *SUPV3L1* gene.

2 | RESULTS

2.1 | A neurodegenerative disease with characteristic non-neurological findings

2.1.1 | Case 1

The proband (Figure 1A: III.3) is a 13-year-old male child who was born to a G3P2, 29-year-old, healthy mother. Pregnancy was unremarkable and delivery was at full term by cesarean section, no resuscitation was required and APGAR scores were 9 and 10 at 1 and 5 minutes, respectively. The child's birth weight was 3.1 kg and he was discharged home with no immediate neonatal concerns. He continued to have normal early development as he was sitting independently by age of 6 months. At the age of 10 months he started to pull up to stand. His physical examination at the age of 10 months was unremarkable apart from fair skin and hair compared to his parents, but his eye examination showed photophobia, blepharitis, corneal erosions, light colored iris, hypopigmented fundus, peri-papillary atrophy, and reddish foveal reflex. He did not gain any further skills until the age of 2 years when he started to deteriorate and lost the ability to pull up to stand, and was able to sit up for shorter periods. His physical examination was remarkable for hypertonia and hyperreflexia and eye examination revealed significant astigmatism with poor attention. The anterior segment showed blepharitis, severe meibomitis, mild conjunctival hyperemia, moderate waxy pallor of the optic disc, and retinal pigmentary changes, while the macula reflex was dull with no pigmentary changes at the fovea. He continued to have progressive lower limb spasticity since then. By the age of 4 years, he showed minimal improvement when he was able to sit without support and crawl, and occasionally stand for a brief time. Around that time as well, he was able to identify a few colors, tried to draw circles and trace dashes, but pencil handling was very weak. He worsened again by the age of 5 years and since then he was only able to sit with support for short periods. He could not hold pencils and was only able to reach and hand-grasp large and

(A)

(B)

(C)

(D)
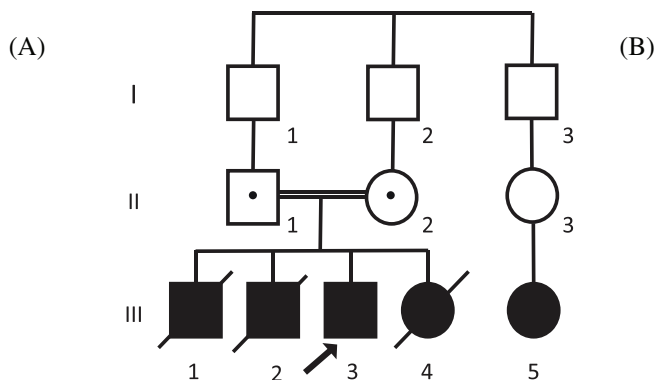
FIGURE 1 A neurodegenerative disease with characteristic extra neurological findings. (A) Family pedigree illustrating the autosomal recessive inheritance and, where known, the carrier status of parents. Ages of death for the three deceased siblings are: 5 years (III.1), 18 months (III.2), and 3 years (III.4). (B) Extensive area of vitiligo visible on the proband (patient III.3). (C) Selected MR images for the proband (patient III.3). Left panel: Sagittal T1 weighted image at the midline age of 5 years showing atrophy of the optic chiasm (thin white arrow) and atrophy of the pons (thick white arrow). Mild volume loss noted also in the midbrain. Middle panel and Right panel: Axial T2 images at the level of the basal ganglia at age of 27 months and 5 years, respectively showing normal volume and signal intensity of the basal ganglia with age-appropriate myelination. (D) CT and MR imaging of the proband's younger sister (patient III.4) were performed at age of 22 months. Left top panel: axial CT image showing focus of calcifications in the left basal ganglia (white arrow). The right basal ganglia calcification is not shown here. Right top panel: midline sagittal T1 weighted image demonstrates atrophy of the optic chiasm and the pons, similar to patient 1. Bottom left and right panel: Axial T2 and FLAIR weighted images, respectively: there is volume loss of the putamina with focal areas of increased T2/FLAIR signal intensity (black arrows in bottom left panel). Delayed myelination is seen in this patient as demonstrated in T2 weighted image
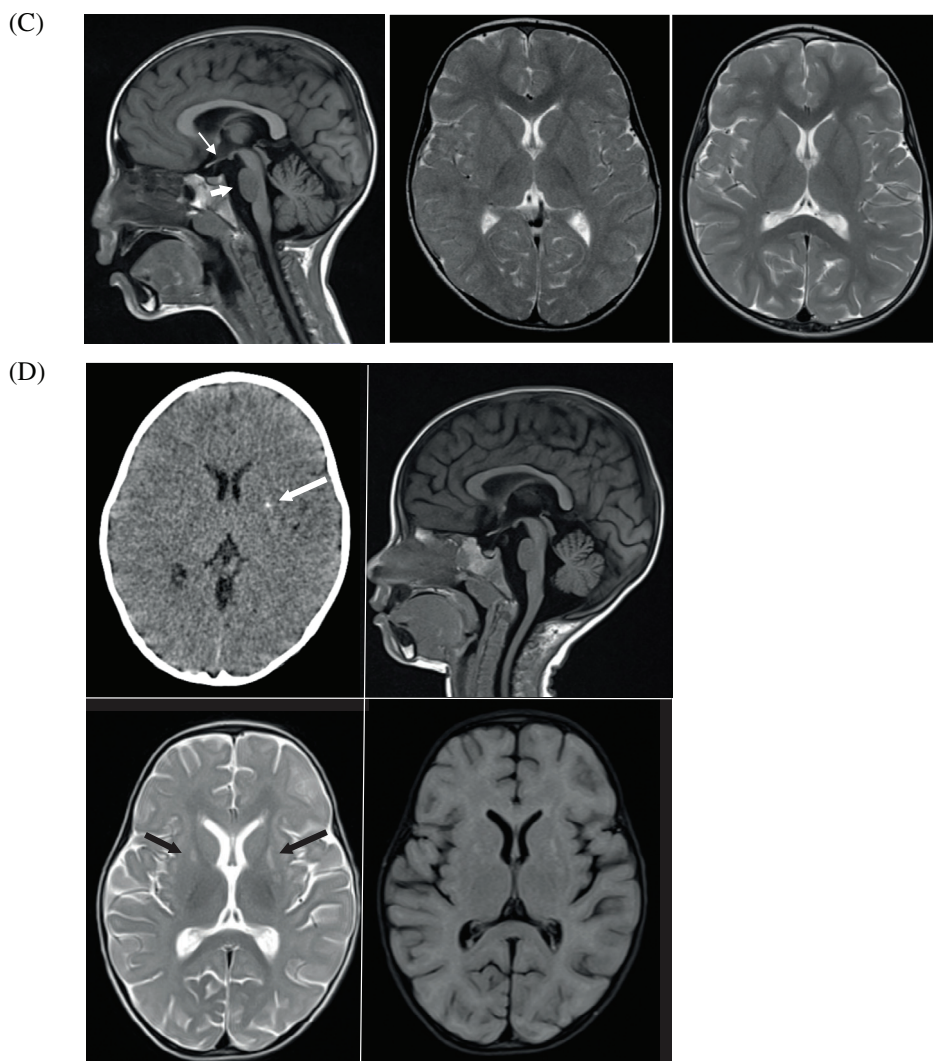
light objects. By the age of seven, his night vision was worsening and eye examination showed worsening blepharitis, superficial corneal erosions, optic disc pallor, diffuse retinal nerve fiber layer atrophy, dull macular reflex, and more marked generalized retinal pigmentary changes. He continued to have progressive lower limb spasticity and started to have hypopigmented skin patches mainly over his extensor joint surfaces and was diagnosed with vitiligo. At the age of 10, he was able to hold pencils again and write simple words. His vitiligo was more extensive and covered large areas of his body and he started to have silver-gray hair. His severe

photophobia continued and he continued to show blepharitis with diffuse superficial corneal erosions, and diffuse pallor of the optic disc with arteriolar attenuation. With regards to language development, at the age of 1 year, he had a few words with meaning but lost all of his vocabulary at the age of 3 years and still is nonverbal. However, his nonverbal intelligence was relatively preserved and demonstrates a relatively good understanding of verbal commands, ability to write his name and a few other words and engage into discussions by nonverbal clues. Intelligence quotient (IQ) test performed at the age of 12 years and 7 months showed full scale IQ of 53. He has a friendly predisposition and enjoys looking at and playing with other children. However, he developed manipulative behavior, sensitivity, and sadness about his overall condition and excessive stubbornness at times. He is still able to take regular family food but with increasing difficulty and poor oral intake. There is no history of seizures or jaundice. He was admitted four times during early childhood for acute gastroenteritis at ages of 6, 9, 12, and 13 months and at the age of 7 years with bronchopneumonia.

The last physical examination at the age of 12 years was remarkable for growth deficiency and microcephaly (weight at −5.2 SD, height at −3 SD, and head circumference at −2.5 SD). He was sitting in a wheelchair and was able to support his head for short periods. He was keeping his eyes closed and tilting his head to see because of severe photophobia. He was smiling and cooperative and able to remember health care team members. He had no dysmorphism apart from long eye lashes and synophyrus. His skin is fairer in complexion since birth compared to his parents and he had extensive areas of vitiligo that were covering large areas of his trunk (Figure 1B) and extremities as well as patches of silver hair. He had dry skin around his mouth and eyes. He had pectus excavatum. There was no hepatosplenomegaly. He had generalized muscle wasting with spasticity over his four limbs, brisk deep tendon reflexes, and contractures at the ankles.

Laboratory investigations showed intermittent elevation of lactate, highest recorded was 4.6 mmol/L. Full blood count was normal apart from intermittent thrombocytosis. Liver function test, creatine kinase, alkaline phosphates, calcium and phosphate, thyroid stimulating hormone, and free thyroxine were all normal. Serum uric acid was mildly low at 0.14 mmol/L (normal 0.2-0.45). Acylcarnitine profile and urine organic acids were normal. Plasma amino acids showed normal alanine, elevated proline, and low branched chain amino acids. Chitotriosidase in plasma was elevated at 3.0 nmol/min/mL (normal <1.5), he had normal urine oligosaccharides and sialic acid and low galactose-

6-sulfate sulfatase activity of unknown significance. Congenital Defects of Glycosylation screen by transferrin isoforms in serum by HPLC as well as by isoelectrofocusing yielded a normal pattern. Oxidative phosphorylation enzymology in skin fibroblasts was normal.

MR imaging of the brain was performed at the age of 27 months and 5 years (Figure 1C). There was mild atrophy of the optic chiasm. Atrophy of the pons was noted with flattening of the anterior pons. The anteroposterior diameter of the pons was below the third percentile at the age of 5 years.[18] The anteroposterior diameter of the pons did not show any interval growth between the two scans. Mild volume loss of the midbrain was observed without significant cerebellar atrophy. The scans showed otherwise age-appropriate myelination without any white matter signal abnormality. The basal ganglia were normal and there were no areas of abnormal diffusion restriction. Nerve conduction velocities study at the age of 2 years was normal as well as Brainstem Auditory Evoked Potentials. Echocardiography at the age of 10 years was normal.

2.1.2 | Case 2

The second patient was the younger sister (Figure 1A: III.4) of the proband and passed away at the age of 3 years. She had unremarkable perinatal history and no early infancy concerns. When she was first assessed at the age of 10 months, there was evidence of moderate global developmental delay as she was able to support her head and roll over but was not sitting up yet. At the age of 22 months, she was able to sit independently, crawl, pull up to stand, and hold onto furniture. She was also able to reach for toys, transfer objects across the midline, and say baba and mama specifically. She had a febrile illness at the age of 22 months after which she lost all her developmental milestones including head support. She was spastic and had wondering eye movements. She had a slow recovery thereafter and at the age of 30 months she was able to stand with support and to cruise around the furniture. She regained her ability to hold and transfer objects and said baba and mama specifically with no other words. Physical examination at 30 months was remarkable for significant failure to thrive and microcephaly (weight at −5 SD, height at −3 SD, and head circumference at −4.6 SD). She had no dysmorphic features and positive findings included fair skin complexion, mild pectus excavatum, and increased peripheral tone with normal deep tendon reflexes. Biochemically, she had normal lactate 1.8 mmol/L, elevated ALP of 725 U/L, and borderline elevation of AST 39 U/L. There was no suggestion of photophobia and eye

examination showed mild disc pallor, mild attenuation of vessels, pigmentary changes at macula, and dull foveal reflex. CT scan showed bilateral foci of calcifications in the putamina. MR imaging of the brain revealed delayed myelination at age of 22 months. The putamina showed volume loss and foci of T2/FLAIR hyperintensity. Similar to patient 1, there was atrophy of the optic chiasm and the pons. There were no areas of abnormal diffusion restriction (Figure 1D). EEG during the admission with neuroregression was normal in terms of background and epileptic activity. At the age of 3 years, she developed a choking episode with a grape that led to suffocation and profound hypoxic ischemic injury and she died a few weeks later.

2.1.3 | Family history

The two siblings were born to first-cousin parents of Omani Arab ethnic origin. They had two older brothers who passed away at the ages of 5 years and 18 months, respectively (Figure 1A: Individuals III.1 and III.2). The older brother (III.1) had never gained any development since birth including social smiling and head support. He also had seizures and was very spastic. He was diagnosed with systemic lupus erythematosus (SLE) a few months prior to his death at the age of 5 years with chest infection. The second brother (III.2) had a very similar course of absence of any developmental gain and progressive spasticity. He had no seizures until the time he passed away at 18 months old with a chest infection. Both children were described to have fair hair and skin compared to parents and other family members.

A female cousin on both sides (III.5), who was 10 years old when first seen, had severe global developmental delay with absent head support, seizures, and spasticity. She currently is 15 years old, is bed-bound, extremely spastic, and scissoring, but understands conversations, smiles, and can point to her needs. She also has a fair skin color but her mother has fair skin color too, making it difficult to conclude this is a key diagnostic feature.

2.1.4 | Genetic diagnosis

To identify the genetic cause for the disease, also taking into consideration that the parents were first cousins, the proband's DNA was analyzed using exome sequence analysis.

This identified a single and likely deleterious homozygous variant in the *SUPV3L1* gene; chr10:g.70968645C>T; NM_003171.3: c.2215C>T resulting in a premature stop codon (p.Gln739*), classified as a variant of uncertain significance according to ACMG guidelines (PMID: 25741868).

Both the proband and his younger sister were confirmed to be homozygous while both parents were found to be a carrier of this variant. No DNA for testing was available from the deceased older siblings while the female cousin is unavailable for testing. The entire exome sequencing data of the proband have been investigated in detail for candidate variants, not only for a presumed mitochondrial disease, but also for variants that may explain parts of the clinical symptoms, but this did not reveal any other candidate causal variants.

2.2 | C-terminal region of SUPV3L1

The biological importance of the 47 amino acid (aa) C-terminal region (aa 739-786) that was missing in the patients as a consequence of the identified homozygous *SUPV3L1* nonsense mutation (Figure 2A) is unclear, although two potential functions have been published, namely interaction with RNA[28] and interaction with the Ragulator complex protein LAMTOR5.[27] The 650 to 786 region, described to interact with LAMTOR5,[27] is larger than the region missing in the patients (Figure 2B), so it is uncertain if the last 47 amino acids are essential for binding. The 737 to 777 region that is described as potentially RNA-interacting is contained within the last 47 amino acids (Figure 2B), but was identified with a genome-wide screen and not confirmed with small scale targeted experiments.[28]

In order to further investigate the importance of the missing C-terminal region, we examined its evolutionary conservation using Jackhmmer.[20] Starting with the C-terminal region (residues 650-786, the region that has been reported to interact with LAMTOR5), iterative homology detection was performed against the eukaryotic sequences in the reference proteomes database, until convergence (four iterations) using default cut-offs (Figure 2B). We only detected homologs in bilaterian species for that region. Further inspection revealed that these homologs were all SUPV3L1 orthologs. Interestingly, the C-terminal region contains a predicted conserved double amphipathic helix (JPred4,[22] DeepCNF[23]) flanked by disordered regions (IUpred2[24]; Figure 2B,C). The double helix co-localizes with a predicted ANCHOR binding site (IUpred2[24]), defined as a region that has to be able to form a favorable interaction with a binding surface of an ordered protein and is embedded in a disordered environment. Taken together we found that some of the residues missing in the patients' truncated SUPV3L1 protein are well-conserved and can form a helix or interaction site.

The RRKK stretch at the end of the C-terminus is slightly conserved and resembles a nuclear localization
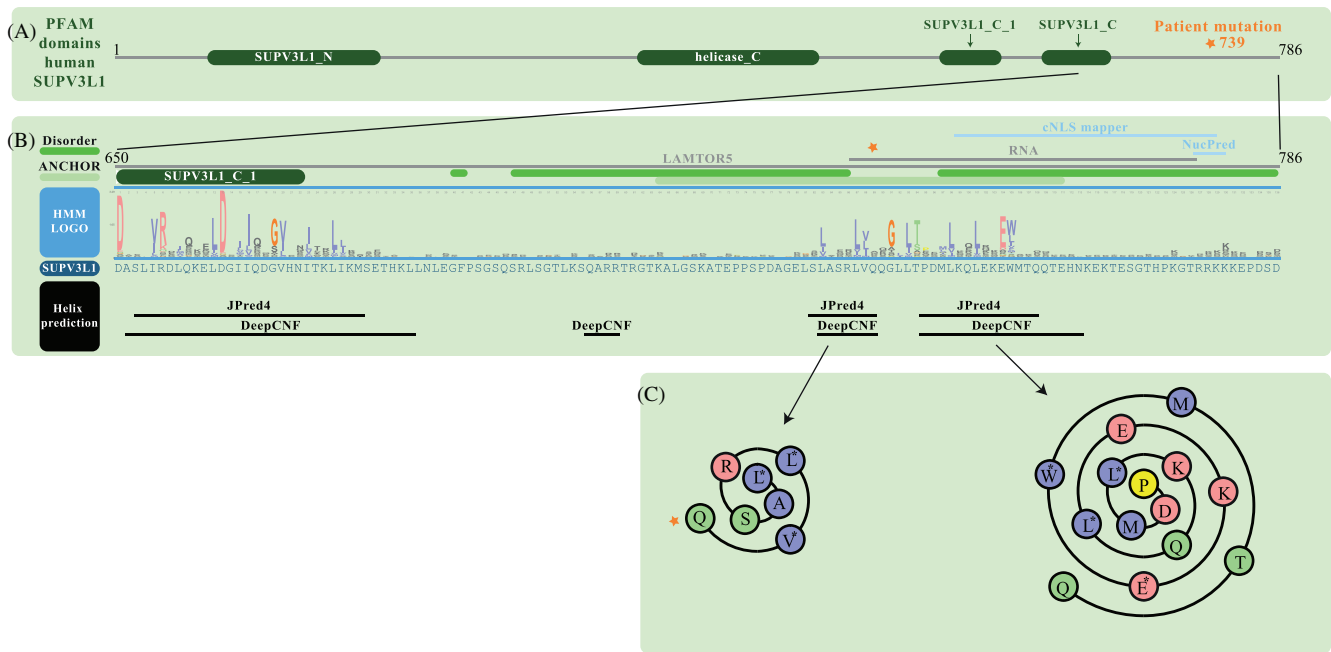
FIGURE 2 Conservation of the C-terminal region missing in the patient. (A) Domain structure of the human SUPV3L1 protein.[19] (B) The 650 to 786 amino acid region of human SUPV3L1. A Hidden Markov Model was created by a Jackhmmer[20] search with the 650 to 786 amino acids region, the reference proteome database and four iterations. The sequence conservation was visualized using the online available Skylign tool.[21] Underneath the profile the human SUPV3L1 amino acid sequence is shown as well as the predicted helical secondary structure according to JPred4[22] and DeepCNF.[23] Above the logo specific regions were indicated, namely domain regions (Pfam[19]), disordered regions (IUpred2[24]), ANCHOR binding sites (IUpred2[24]), regions important for nuclear localisation (NucPred[25] and cNLS mapper[26] with standard settings) or interaction with LAMTOR5[27] or RNA.[28] (C) Predicted helical regions identified in Figure 2B by both tools were visualized in a wenxiang plot[29] using the R package helixvis,[30] conserved residues (HMM logo from Figure 2B) are indicated with an asterisk. Position of the preliminary stop-codon mutation of the patient is in all figures highlighted with an orange star. Amino acid residues are colored according to the ClustalX coloring scheme with glycine in orange, proline in yellow, small or hydrophobic amino acids in purple, hydroxyl or amine amino acids in green, charged amino acids in red, and histidine or tyrosine in blue

signal (NucPred,[25] cNLS mapper[26]). This region was also lost by the truncation.

2.3 | Expression of the truncated protein

SDS-PAGE and Western blot analysis showed that the truncated protein is formed (Figure 3A), although the intensity of the truncated SUPV3L1 protein in patient fibroblasts was only a fraction (12%, P-value = 0.015) of the intensity of full-length SUPV3L1 in controls. Reduced RNA levels could provide one possible explanation for reduced truncated protein levels, although there is no reason to suspect nonsense mediated decay, as the new stop codon lies in the last exon of the gene. Indeed, quantitative RT-qPCR experiments showed that the *SUPV3L1* transcript level was slightly but not significantly higher in patient compared to control fibroblasts (Figure 3B).

To further investigate the phenotype of patient fibroblasts vs control fibroblasts and to determine if potential differences are caused by the *SUPV3L1* mutation, we used lentivirus transduction to create both patient and control stable fibroblast lines (co-)expressing either the cDNA for a control protein (green fluorescent protein [*GFP*]) or full-length *SUPV3L1*. RT-PCR amplification over the mutant site and subsequent sequence analysis showed that the wild-type transgene was expressed in the complemented patient fibroblasts (Figure 3C). Expression was confirmed by Western blot analysis (Figure 3D), showing that in the complemented patient cell line, full-length SUPV3L1 was present, but at much lower levels (24%, P-value = .003) compared to the GFP-complemented control line (Figure 3D). The *SUPV3L1* lentivirus-treated control fibroblasts showed increased full-length SUPV3L1 levels (335%, P-value = .055) compared to the *GFP* control. Western blots were in addition probed for ACTIN as loading control and for the SUPV3L1 interaction partners PNPT1 and GRSF1 (Figures 2D and 3A).

2.4 | mtDNA copy-number

As the lack of SUPV3L1 was previously shown to decrease mtDNA copy-number in mice, HeLa, and
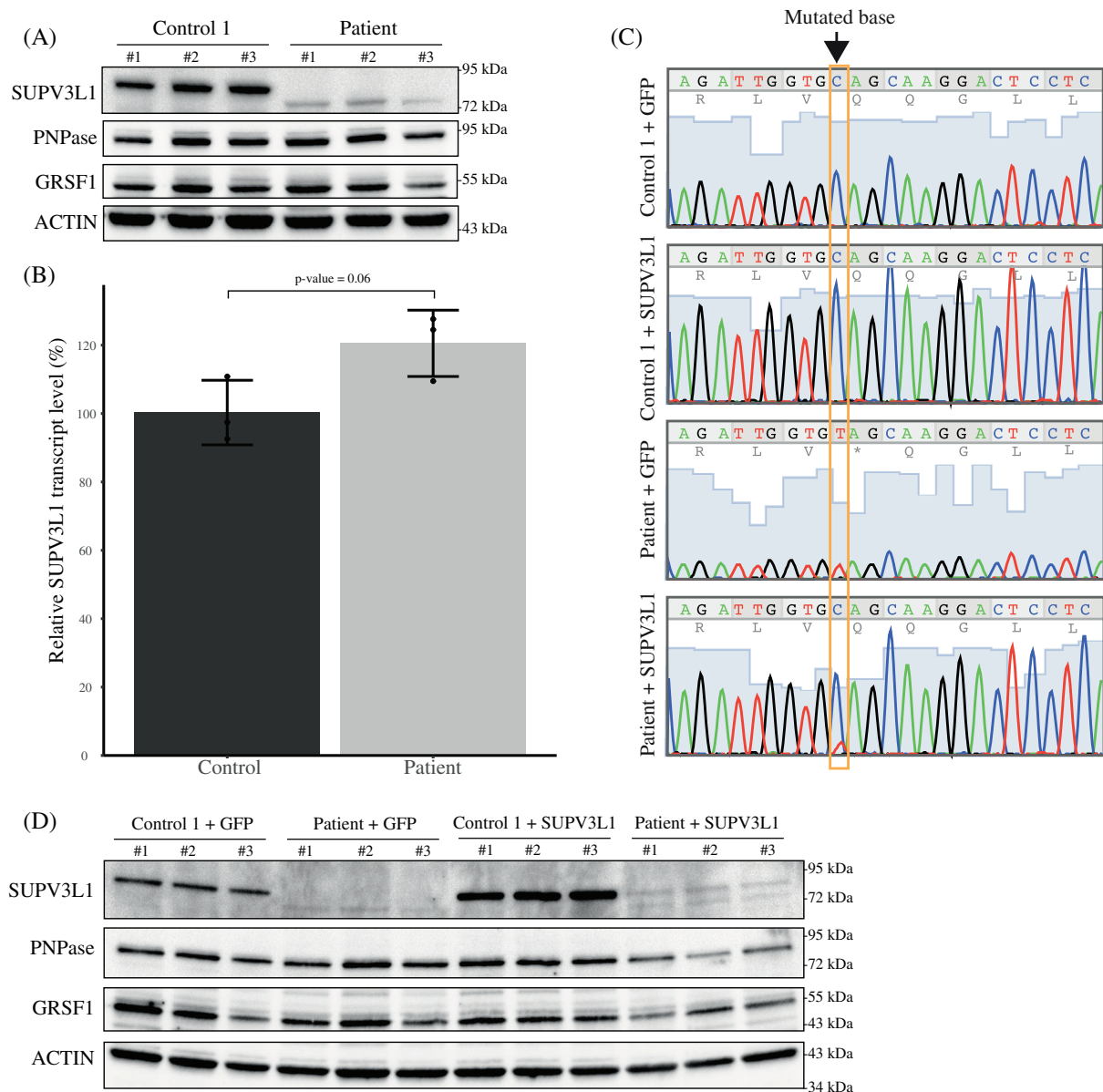
FIGURE 3 Construction and characterization of the fibroblast cell lines. (A) Cropped images of a representative Western blot with lysates of control 1 and patient fibroblasts ($n = 3$) probed for SUPV3L1, PNPase, GRSF1, and ACTIN. SUPV3L1 shows in controls a larger band for full-length SUPV3L1 (~88 kDa) and in patients as predicted a smaller band of ~73 kDa for truncated SUPV3L1. (B) Relative *SUPV3L1* transcript levels in control and patient fibroblasts ($n = 3$). Individual data points are indicated and error bars show $\pm$ standard deviations. *P*-value is based on a two-sample *t*-test. (C) Sequencing results obtained with the R_SUPV3L1_2362 primer ($n = 1$) are shown as a 24-base window with the patient mutation on position 10 (corresponds with position 2215 in reference cDNA sequence of *SUPV3L1* CCDS7287.1). Blue bars represent the sequencing quality, each base is shown in its own color (A = green, G = black, T = red, and C = blue) and encoded amino acid sequence is indicated in light gray below the DNA sequence. (D) Cropped images of a representative Western blot with lysates of the fibroblasts supplemented with either the *GFP* or the *SUPV3L1* gene ($n = 3$) probed for SUPV3L1, PNPase, GRSF1, and ACTIN. Images of entire blots are available in the source file

Osteosarcoma cell lines,[17,31,32] we investigated the copy-numbers in patient and four control fibroblast lines. The mtDNA levels observed in patient fibroblasts were comparable with the levels measured in the control fibroblasts (Figure 4).

2.5 | mtRNA processing

In order to investigate processing of light-strand templated mtRNAs, in which mtEXO plays an important role,[7,8,10] RNA isolated from patient and control fibroblasts as well as
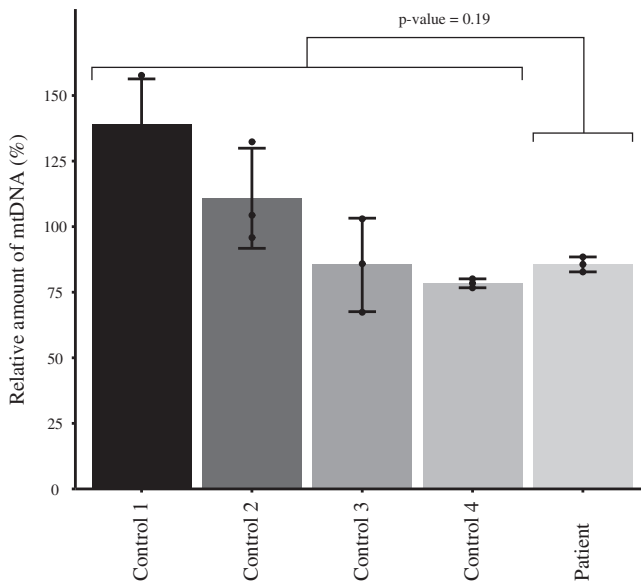
FIGURE 4 Mitochondrial DNA copy-number in patient fibroblasts. The copy-numbers, which were calculated from total fibroblast DNA qPCR measurements ($n = 3$), are shown relative to the mean of control fibroblasts. Individual data points are indicated and error bars show $\pm$ standard deviations. Statistics used a two-sample t-test to compare patient copy-numbers with the copy-numbers of all controls together

the complemented lines was analyzed by Northern blots to visualize processing intermediates. Probing the blot for *ND6* showed three distinct bands in all tested cell lines (Figure 5A), two precursor *ND6* RNA species and the mature *ND6* (Figure 5B), based on our previous assignment in U2OS cells.[33] Compared to controls, the mature *ND6* transcript showed a clear reduction in the patient cells. This was further quantified by calculating the ratios of mature *ND6* over the two precursor RNA species (Figure 5C), showing a statistically significant reduction of mature/immature ND6 ratios in the patient cell line. This difference between patient and control ratios was also observed in the *GFP* complemented lines. In the *SUPV3L1* supplemented patient cell line the ratio between *ND6* and pre*ND6*-2 was significantly increased compared to the *GFP* supplemented patient line, from 0.47 to 0.92, suggesting that the low mature *ND6* levels in the patient cell line are caused by the absence of full-length *SUPV3L1*. The ratio of *ND6* over pre*ND6*-1 showed a similar trend but this was not statistically significant. The ratios between the two precursors did not show any significant difference between patient and control lines (not shown). In conclusion, the levels of mature *ND6* compared to its precursors were lower in the patient fibroblasts and addition of full-length *SUPV3L1* partly restored this. We did not observe evidence of extensive accumulation of RNA breakdown products as were observed previously with for example *GRSF1* knockdown

in U2OS cells.[33] The blots were in addition probed for mitochondrial *12S* and nuclear *18S* ribosomal RNAs to demonstrate equal loading (Figure 5A).

2.6 | dsRNA accumulation

Loss of mtEXO by RNAi mediated depletion of its components, including SUPV3L1, has previously been shown to result in the accumulation of dsRNA and RNA:DNA hybrids.[17] To determine whether the patient cell line showed a similar phenotype we examined the accumulation of dsRNA in patient and control cells by immunofluorescence, using the dsRNA specific J2 antibody and an antibody against SUPV3L1 (Figure 6). SUPV3L1 immunofluorescence shows a weak but clearly detectable mitochondrial SUPV3L1 signal in control cells, whereas the patient cells show mostly background fluorescence. The loss of the full-length SUPV3L1 protein and the greatly diminished levels of the truncated form of the protein, as observed by Western blot analysis, are consistent with these observations. The SUPV3L1 complemented patient fibroblasts showed very little improvement of the SUPV3L1 signal in agreement with its low level of expression that we observed also by Western blot analysis. Occasionally, but not in more than a few percent of all cells, we did observe cells with a clear mitochondrial SUPV3L1 signal. A majority of patient cells showed accumulation of dsRNA visible by J2 detected punctae ($62 \pm 4.9\%$ for *GFP* complemented patient cells), whereas these were rarely detected in control cells. Despite the low levels of SUPV3L1 expression in the complemented patient cells, the number of cells that were clearly positive for dsRNA were significantly reduced compared to the *GFP* complemented cells ($24 \pm 0.58\%$, $P < .002$), showing that the loss of full-length SUPV3L1 is the principal cause of this cellular phenotype in patient fibroblasts.

3 | DISCUSSION

Here, we report for the first time two sibling patients with a homozygous mutation in the *SUPV3L1* gene. The two patients showed a consistent clinical phenotype of global developmental delay, neuroregression, progressive spasticity, growth restriction, retinal dystrophy, optic nerve atrophy, fair skin complexion, and possible link to autoimmune disease (vitiligo and SLE). The proband had persistent severe photosensitivity with corneal erosions noted as early as 10 months of age. Characteristic MRI features included atrophy of the optic chiasm and the pons. Basal ganglia calcifications and atrophy of putamina were additional important findings in the
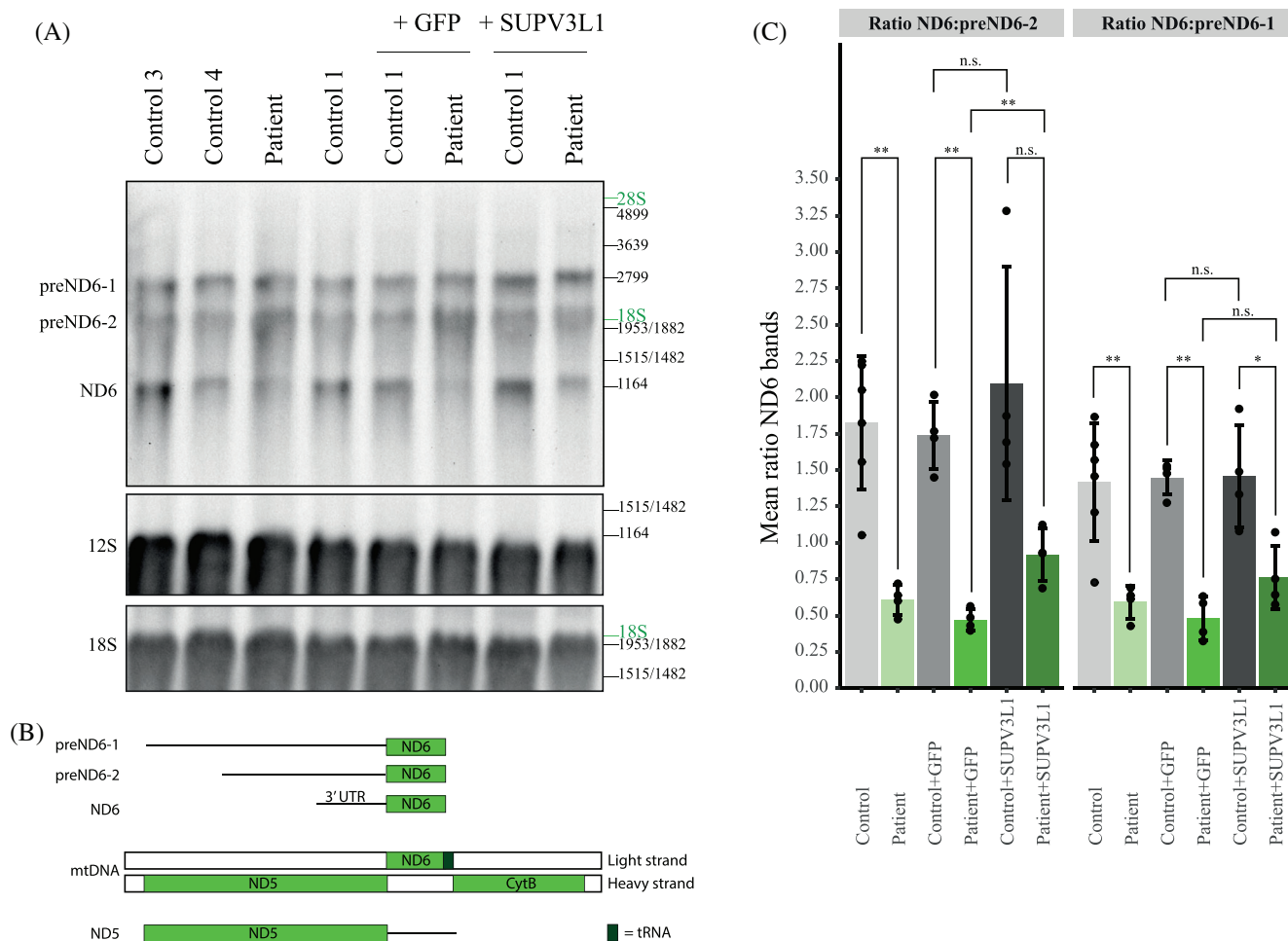
FIGURE 5 Processing of the light-strand *ND6* transcript in patient fibroblasts. (A) Cropped images of one representative Northern blot probed for *ND6*, *12S*, and *18S*. Images of the entire blot and of three biological repeats are available in the source file. Position of the DNA marker bands are indicated as well as the position of the 18S and 28S rRNA (indicated in green). Precursor *ND6* species are indicated with "pre." (B) Schematic representation of the three ND6 bands visible on the northern blot of Figure 5A. The ND5 transcript is in addition shown as it is similar in size as preND6-1 and can be stained by the ND6 probe as it contains ncND6. (C) Ratio's between the quantified mature *ND6* and its precursors bands ($n = 4$, except for control where $n = 6$ composed of $n = 4$ control 1 and $n = 1$ of control 3 and 4) were calculated. Statistics used two-sample t-tests, error bars indicate $\pm$ standard deviations and individual data points are shown. Outcome of the statistical tests are indicated as nonsignificant (n.s.), P-value $\leq.05$ (*) and P-value $\leq.01$ (**). Exact P-values are available in the source file

younger sister (Figure 1D). Similar to other mitochondrial leukoencephalopathies, the developmental delay is of variable severity and age of onset, with characteristic periods of acute and subacute neurological deterioration with subsequent variable periods of stabilization or partial recovery. The neuroregression episodes on some occasions were linked to intermittent illnesses but had no obvious trigger on other occasions. The relationship of autoimmune dysfunction with *SUPV3L1* related mitochondrial disease is evident through the early onset and extensive vitiligo in our proband and the severe SLE in his older deceased sibling. Autoimmune diseases, such as vitiligo, may have an innate immune component (eg, Reference 34). Knockdown of the mitochondrial degradosome enzyme PNPase and SUPV3L1 results in clear accumulation of mitochondrial dsRNA, but only for PNPase has it been related to leakage of mitochondrial RNA into the cytoplasm and triggering of an innate type I interferon immune response.[35] The limitation with these observations is that they were obtained with HeLa cells. Mouse knockout models for *SUPV3L1* showed that a full knockout is embryonic lethal while various conditional knockouts show variable but severe phenotypes.[36,37] Of particular interest is a severe skin phenotype with persistent inflammation that curiously presented itself in a conditional knockout with a Cre recombinase that was under the control of a normally silent *Mx1* promoter and is inducible by interferon alpha, interferon beta, or synthetic double-stranded RNA.[36] However, the authors did not use any inducing agent to create
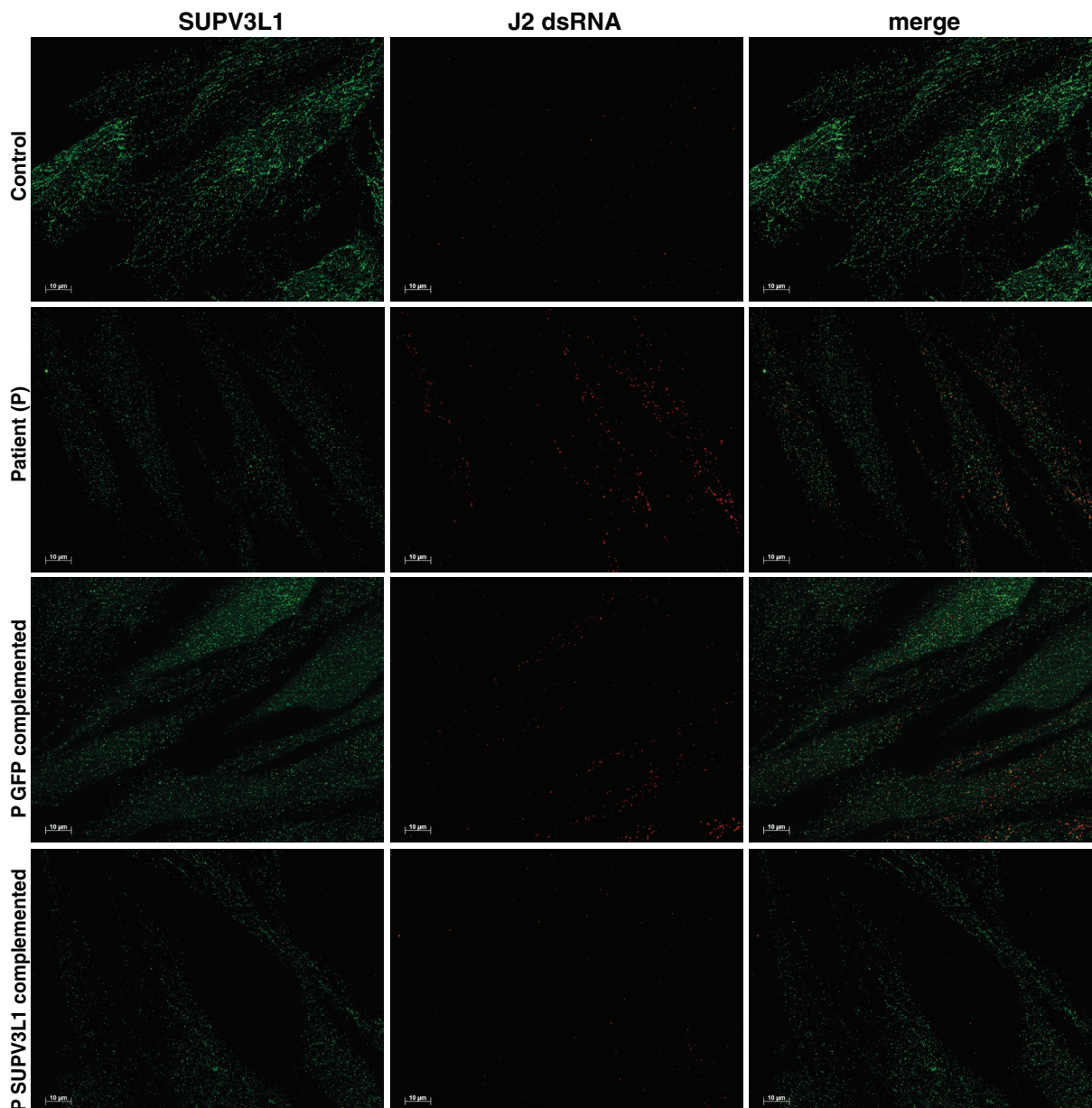
FIGURE 6 Double-stranded RNA levels in patient fibroblasts. Control and patient fibroblasts, as well as lentiviral *GFP* or *SUPV3L1* transduced fibroblasts (as indicated) were stained for SUPV3L1 (green) and the dsRNA detecting J2 antibody (red)

the severe phenotype, nor was the involvement of the degradosome in preventing mitochondrial dsRNA escape known in 2009. The authors therefore speculated that there might have been promoter leakage or inadvertent promoter activation by endogenous interferon production. What is particularly interesting is that the authors discuss a feed-forward amplifying loop as they were very surprised by the severity of the phenotype under the *Mx1* promoter and the extent of *SUPV3L1* deletion. We can therefore speculate that *SUPV3L1* deletion/dysfunction in other cell types than HeLa cells or in certain tissues could elicit dsRNA escape with concurrent Mx1 promoter activation, thus explaining the results from this mouse

model. Unfortunately, we could not reliably detect IFNB1 mRNA in fibroblasts, caused by very low or absent expression, and therefore could not determine whether an innate immune activation is occurring in the patient fibroblasts. Arguably, fibroblasts are not an appropriate model system to test this response. It would be very interesting to revisit the above mouse model and test for innate immune activation.

Although the two older siblings (III.1 and III.2) who passed away had progressive spasticity and fair skin color that made it likely that they were similarly affected with *SUPV3L1*-related mitochondrial disease, they have remarkable differences in showing no gain of

developmental milestones rather from the beginning. There was no DNA available from them and their *SUPV3L1* status is not known. It is uncertain if they represent a wide range of presentation related to *SUPV3L1* related disease, or they had an additional neurodevelopmental disease that masked the *SUPV3L1*-related presentation or if they had a different diagnosis altogether. Exome sequence analysis of the proband identified a single homozygous truncating mutation in the proband. Further genetic testing identified the same homozygous mutation in the deceased younger sister, while both parents were carrier. Even though further analysis of the proband's exome did not identify any other candidate causal variants, we cannot exclude other causal variants in the noncoding part of the genome.

We studied the mutation in a patient derived fibroblast cell line to determine if the mutation causes a mitochondrial gene expression defect and might be the underlying cause of the patient's disease. The last, however, is difficult to extrapolate from the fibroblast model as the *SUPV3L1* expression levels in tissues varies,[38] the mitochondrial phenotype in fibroblasts was very mild, with normal mtDNA levels and no detectable oxidative phosphorylation defect. In addition, we did not study any possible nuclear consequences that might be anticipated for a protein that is normally found in both the mitochondrial and nuclear compartment.[16]

In theory the preliminary stop-codon would result in the expression of a C-terminally truncated protein that misses a disordered region, but has not lost the in Pfam[19] annotated N-terminal domain, the helicase domain and the two additional C-terminal domains (Figure 2A). We show that parts of the lost disordered region are conserved (Figure 2B) and potentially form two conserved amphipathic helixes (Figure 2C). In addition, a previous report has shown interactions of the SUPV3L1 C-terminus with RNA[28] and LAMTOR5.[27] The RNA interacting region was demarcated by amino acids 737 to 777[28] and part of the observed conserved residues (Figure 2B) fall into the reported region. This strengthens the hypothesis that the C-terminal has a biological function, although there is no obvious relationship with the presence of an amphipathic helix, suggesting interaction with a membrane, and an interaction with RNA or LAMTOR.

We[39] and others[40-44] speculated previously that evolutionary changes in the organization of the mtDNA required additional mitochondrial proteins for normal gene expression. The human SUPV3L1 helicase has all reported catalytic domains found in its yeast ortholog,[38] while we find the C-terminal disordered region with amphipathic helixes only in Bilateria. The tRNA punctuation gene order, with the processing of RNA being

dependent on the position of the tRNA genes, evolved as well in Bilateria.[45] We therefore speculate that the C-terminal region of SUPV3L1 evolved in Bilateria to allow proper processing of mtRNA with the new gene order.

A shorter variant of SUPV3L1 with a size predicted for the truncated protein was detected by Western blot analysis (Figure 3A). The expression was however low compared to the expression of the full-length protein in control fibroblasts, while the transcript levels were normal (Figure 3B). This suggests that the truncated form might be less stable. Of note for this conclusion is the assumption that the polyclonal SUPV3L1 antibody recognizes the same epitopes on the truncated protein as on the wild type protein. The immunogen used to create the antibody spans the region 441 to 786 of SUPV3L1, so in theory antibodies specific for the region 739 to 786, which is missing in the patient, can be present and contribute to the detection of the full-length protein. Low intensities were however also observed in the complemented patient cell line for full-length SUPV3L1 (Figure 3D) containing all possible antibody binding sites. A more likely explanation for the lower SUPV3L1 intensities observed in the patient is therefore instability of the protein. Possibly the levels of the full-length SUPV3L1 in the complemented fibroblasts are low due to interference of the still present truncated protein with mtEXO formation, thereby also destabilizing the full-length protein. Inefficient lentiviral transduction is unlikely to be the cause as the transduction was performed twice and, in both instances, a low full-length SUPV3L1 expression was observed in patient cells (data not shown), whereas in control cells transduced with the *SUPV3L1* cDNA, protein expression was increased more than three-fold compared to nontransduced and *GFP* transduced cells.

On northern blots (Figure 5) the ratios between mature and precursor *ND6* indicated a defect in light-strand RNA processing. Although we did not observe the strong accumulation of *ND6* containing transcripts that was previously reported by Jourdain et al[8] upon depletion of *SUPV3L1*, our observations of a reduced amount of mature *ND6* compared to its precursors (Figure 5) matches with the *SUPV3L1* depleted northern blot of Jourdain et al fig. 7D lanes 1 and 2.[8] Similarly, Matilainen et al[46] have described a compound heterozygous mutation in the SUPV3L1 mtEXO partner protein PNPT1, in a child with Leigh syndrome, and demonstrated an *ND6* processing defect with reduced mature *ND6* mRNA. Improper processing of noncoding RNA could lead to accumulation of dsRNA as the noncoding RNA is the reverse complement of the heavy strand templated RNA that provides most functional mitochondrial RNA species. This accumulation of dsRNA was previously observed with depletion of full-length

SUPV3L1.[17] Likewise, accumulation of dsRNA was readily observed with immunofluorescence in patient but not in control fibroblasts (Figure 6). Introduction of the wild-type SUPV3L1 in the patient cell line partly restored the *ND6* ratios on Northern blot and lowered the levels of dsRNA detected by immunofluorescence, indicating that the light-strand processing defect is caused by the *SUPV3L1* mutation. It is likely that the low expression levels of full-length SUPV3L1 in the complemented cells were the reason we did not observe complete restoration of the phenotype.

In this report, we focused on the mitochondrial role of SUPV3L1 as the patient showed signs for a mitochondrial defect, including higher lactate levels. Immunofluorescence has shown previously that the protein can be localized to the nucleus,[16] and has a nuclear localisation signal in its C-terminus (amino acids 777-781)[16] that was in addition predicted by NucPred[25] and cNLS mapper[26] (Figure 2B). We show that the RRKK stretch at the end of the C-terminus is slightly conserved (Figure 2B). It therefore might be that the truncated SUPV3L1 protein is distributed differently in the cell than the full-length SUPV3L1. Due to the low protein levels of truncated SUPV3L1 we were not able to determine the subcellular localization with immunofluorescence. It could be that part of the patient phenotype is caused by the absence of the SUPV3L1 protein from the nucleus. Apart from a possible nuclear localization signal, deletion of the C-terminal 136 amino acids also results in less efficient mitochondrial localization,[27] despite the presence of a dedicated N-terminal mitochondrial targeting sequence.[13] Therefore, the truncated patient protein might also be less efficiently targeted to mitochondria, although we do not have any direct evidence that this is indeed the case. The engineered 136AA C-terminal truncation was also suggested to be less stable compared to the full-length protein,[27] which agrees with our findings. One might speculate that partial mistargeting of a truncated SUPV3L1 protein is in part responsible for its lesser stability.

In conclusion, we report two patients with a characteristic neurodegenerative disorder, likely caused by a preliminary homozygous stop codon mutation in the *SUPV3L1* gene. The *SUPV3L1* mutation is responsible for a mitochondrial light-strand RNA processing defect in fibroblast cells. It is unclear whether this is due to the low-level expression of an unstable truncated SUPV3L1 that causes a deficiency of the protein in mitochondria, or if the processing defect is a direct effect of missing the functionality of the C-terminal region. Conservation of the C-terminal region with amphipathic helixes (Figures 1C and 2B) and other reports[27,28] strengthen the hypothesis that the C-terminal region has a function.

4 | MATERIALS AND METHODS

4.1 | Patient family

Written informed consent for diagnostic and research studies was obtained for the subjects in accordance with the Declaration of Helsinki and following the regulations of the local medical ethics committee (Sultan Qaboos University, Muscat, Oman).

4.2 | Cell lines and culture

Fibroblasts from the patient and four controls were grown in Dulbecco's modified Eagle's medium (DMEM; Lonza BE12-604F) supplemented with 10% fetal calf serum (GE Healthcare) in a 37°C incubator at 5% CO_2. Cells were regularly tested for mycoplasma contamination and found to be negative. Using lentiviral transduction, the full-length *SUPV3L1* gene was introduced in both patient and control 1 fibroblasts. To exclude potential confounders due to the lentiviral treatment a control transduction with the *GFP* gene was performed. These fibroblasts supplemented with the *GFP* or full-length *SUPV3L1* gene were cultured with 2 μg/mL Blasticidin (SAS-Invitrogen, ant-bl-1) to select for cells that contain the transduced gene. Two to four days before experiments the Blasticidin was removed by discarding the medium and replacing it with DMEM or lower glucose containing medium "M199" (Pan Biotech, # P04-07050) without Blasticidin.

4.3 | Exome sequencing

Whole exome sequencing was performed as described before.[47,48] In short, exome enrichment was performed using the SureSelect Human All Exon 50 Mb Kit (Agilent, Santa Clara, California). The exome was sequenced on a HiSeq2000TM sequencher (Illumina). The selection of variants was based on the following criteria: >5 variant reads, nonsynonymous coding and splice variants, a frequency of <0.5% in the following databases, dbSNP (v.137), Exome Aggregation Consortium (ExAC) data (http://exac.broadinstitute.org), and an in-house sequence variant database based on data from the same pipeline containing data from > 20 000 exomes. Based on a recessive inheritance model and presumed homozygosity of a causative variant, only a single homozygous candidate variant remained.

4.4 | RNA isolation and reverse transcription

RNA was isolated and reverse transcribed to determine the effect of the preliminary stop-codon in the *SUPV3L1* gene on *SUPV3L1* mRNA stability and to check the sequence and expression of the *SUPV3L1* transcripts from *GFP* and *SUPV3L1* supplemented cell lines. RNA was isolated from fibroblasts by TRIzol (Invitrogen) extraction according to manufacturer's guidelines. A total of 150 to 500 ng of RNA was treated with DNase I Amplification Grade (Invitrogen, 18068015) to remove potential DNA contamination prior to cDNA synthesis using the Super-Script II Reverse Transcriptase (Invitrogen, 18 064 014) according to manufacturer's protocol with random primers (Promega, C1181), dNTP Mix (Promega, U1515) and with 1 μL Recombinant Rnasin Ribonuclease Inhibitor (Promega, N2515) instead of RNaseOUT. All cDNA samples were diluted with nuclease-free water to 7.5 ng/μL (quantitative PCR) or 12.5 ng/μL (sequencing).

4.5 | Quantitative real-time PCR-based analysis (qPCR)

Each 20 μL qPCR reaction consists of 15 ng of cDNA or 25 ng whole cell DNA, 2.5 mM of forward and reverse primers and 1× SYBR Green Master Mix (Biorad). Measurements were performed in triplicate in Hard-Shell 96-Well PCR Plates (Biorad) within the CFX96 Real-Time System (Biorad). The PCR program consisted of an initial denaturation step at 95°C for 10 minutes followed by 40 cycles of denaturation at 95°C for 15 seconds, primers annealing and extension at 60°C for 60 seconds and fluorescence measurements. The program was followed by a melt-curve analysis to confirm the absence of nonspecific amplicons. Primers are listed in Table 1. Relative quantities of the *SUPV3L1* transcripts or mtDNA genes were determined in relation to that of the nuclear reference gene encoding glyceraldehyde-3-phosphate dehydrogenase (*GAPDH*) or amyloid-beta precursor protein (*APP*), respectively. Changes in the levels between patient and control samples were calculated using the $2^{-\Delta\Delta CT}$ method. CT values of technical repeats that varied by more than 0.3 units from the others were removed prior to analysis.

4.6 | SDS-PAGE and Western blot analysis

Cells were harvested and subsequently lysed on ice for 10 min in lysis buffer (50 mM Tris-HCl pH 7.4, 150 mM NaCl, 1 mM EDTA, 1% TX-100, and 2.5 mM PMSF).

TABLE 1 Primers used in this manuscript

Primer	Sequence (5′ → 3′)
F_SUPV3L1L1_RTqPCR	CCTCTGGACAAGAATGAAG TAAAGA
R_SUPV3L1L1_RTqPCR	CTTGGTGGAAGAGACGAGCA
GAPDH_qPCR_FW	GTCTTCACCACCATGGAGA AGG
GAPDH_qPCR_RV	ATGATCTTGAGGCTGTTGT CAT
human APP FW	TTTTTGTGTGCTCTCCCAG GTCT
human APP Rev	TGGTCACTGGTTGGTTGGC
human cytb FW	GCCTGCCTGATCCTCCAAAT
human cytb Rev	AAGGTAGCGGATGATTCAGCC
F_SUPV3L1L1_1819	TGGTTACGCCGATACATCAA
R_attb2_SUPV3L1L1_stop	AGAAAGCTGGGTGCTAGTC CGAATCAGGTTCCTTCTT
F_SUPV3L1_1921	CTAAGCTACCGATTTATGG
R_SUPV3L1_2362	CTAGTCCGAATCAGGTTCC TTC

After a 5 minutes centrifugation step at 4°C, the supernatant was collected as the cellular lysate. From this lysate 45 μg of protein was separated by SDS-PAGE and transferred to a nitrocellulose membrane. The membranes were probed with primary antibodies to proteins of interest; SUPV3L1 (Proteintech, 12 826-1-AP), GRSF1 (Sigma, HPA036985), PNPase (Abcam, ab96176), and Actin (Novusbio, NB600-532H), bound by HRPconjugated secondary antibodies (Vector Laboratories) and detected by ECL in a ChemiDoc instrument (Biorad). Quantification of the SUPV3L1 and Actin bands was performed with the Image Lab 6.0.1 software.

4.7 | Sequencing

A PCR was performed with the primers F_SUP-V3L1L1_1819 and R_attb2_SUPV3L1L1stop (Table 1) on 25 ng cDNA to amplify the region of *SUPV3L1* containing the patient mutation. PCR products were purified by gel electrophoresis and the QIAquick PCR Purification Kit (Qiagen, 28106) according to manufacturer's protocol and 5 to 20 ng was analyzed on a 3730 Sequence Analyzer with the primer F_SUPV3L1_1921 (data not shown, but in line with results from reverse primer) or R_SUPV3L1_2362. Base calling was performed with the ABI basecaller program and visualized using the 4Peaks software. Results were aligned to the reference cDNA sequence (CCDS7287.1).

TABLE 2 Oligonucleotides used for Northern blot probe synthesis

Primer	Sequence (5′ → 3′)	Range mtDNA	Probe length
hND6-F	TCCTCCCGAATCAACCCTGAC	14 261-14 623	363
hND6-F	GGGGTTTTCTTCTAAGCCTTC		
h12S-F	GGTTTGGTCCTAGCCTTTC	652-1156	505
h12S-R	GCTGTGGCTCGTAGTGTTC		
h18S-F	CCGCGCTCTACCTACCTACC	—	482
h18S-R	CTTGGATGTGGTAGCCGTTT		

4.8 | DNA isolation

Total DNA was isolated from fibroblasts using the NucleoSpin Tissue DNA purification kit (MACHEREY-NAGEL GmbH & Co, 740952.50) according to the company's protocol. DNA was diluted with extraction buffer from the kit to 5 ng/μL prior to quantitative real-time PCR-based analysis (qPCR).

4.9 | Formaldehyde agarose gel and Northern blot analysis

RNA was isolated from fibroblasts by TRIzol (Invitrogen) extraction according to manufacturer's guidelines, prepared for loading onto the gel by the addition of 2.4 to 3.4 volumes of RNA sample buffer mix (10 μL formamide, 3.5 μL 37% formaldehyde, 2.0 μL 5× formaldehyde running buffer) and denatured at 65°C for 5 minutes. The denatured RNA samples were chilled on ice for 2 minutes and 0.4 volumes of RNA loading buffer (50% glycerol, 0.1 mM EDTA pH 8.0, 0.25% bromophenol blue, 0.25% xylene cyanol FF and 9.1 μg/mL EtBr in order to visualize 18S and 28S rRNA bands) was added. A DIG labeled DNA ladder (Roche, 11669940910) was prepared using the same protocol. The prepared ladder and 2.7 to 10 μg of RNA samples were loaded on a 1.2% formaldehyde-agarose gel (1.2% agarose (Seakem GTG agarose, Lonza) in 30 mL 5× formaldehyde running buffer (0.1 M MOPS pH 7.0, 40 mM sodium acetate pH 7.0, 5 mM EDTA pH 8.0) and 26.8 mL 37% formaldehyde in a final volume of 150 mL. The gel was run for 4-5 hours at 60 V. For Northern blotting after electrophoresis, the gel was incubated in 0.05 M NaOH for 20 minutes while shaking at RT followed by a 2 minutes autoclaved MQ wash at RT and 30 minutes wash with 20× saline-sodium citrate (SSC) buffer (3 M NaCl, 0.3 M. sodium citrate pH 7.0). Northern blotting was performed overnight in 6× SSC onto a positively charged Nylon membrane (Roche, 11417240001). The blot was cross-linked afterward for 3 minutes at 120 mJ UV-light before probe hybridizations with DIG (digoxigenin) labeled probes according to

Roche protocols. After probe hybridization, the membrane was briefly washed with 2× SSC/0.1% SDS and 2× for 15 minutes at 65°C with 0.5× SSC/0.1% SDS. The incubations of the Northern blots to prepare for immunological detection are performed as described by the DIG Wash and Block Buffer Set manual (Roche, Cat. No. 11585762001) with CSPD ready-to-use (Roche). DIG labeled probes were synthesized using PCR products as template, originally synthesized using human genomic DNA with the oligonucleotides described in Table 2. The DIG labeling reaction used the same oligonucleotides in combination with PCR DIG Probe Synthesis Kit (Roche Cat. No. 11636090910) according to manufacturer's guidelines. Where necessary blots were stripped in between probings using 2× 20 minutes washes in 0.1% SSC/1%SDS at 80°C. Quantification of the Northern blot *ND6* detections was performed with the Image Lab 6.0.1 software.

4.10 | Immunofluorescence

Immunofluorescence staining was done essentially as described in Hensen et al.[33] For counting dsRNA positive cells in *GFP* or *SUPV3L1* complemented patient cells, we randomly and automatically collected multiple images using a 4 × 4 grid, and counted the number of cells by counting nuclei stained with DAPI, and the number of J2 positive cells based on the J2 antibody staining for three grids of each cell line.

4.11 | Statistics and tools used

Plots, statistics, and calculations were performed with the R statistical package[49] and additional packages gplots,[50] ggplot2,[51] scales,[52] reshape,[53] and helixvis.[30] All statistical test performed in this study are two-sample *t*-test.

CONFLICT OF INTEREST
The authors declare no potential conflict of interest.

AUTHOR CONTRIBUTIONS
Fathiya Al-Murshedi, Eiman Al-Ajmi, and Sana Al-Zuhaibi first examined the patients and performed medical and laboratory tests. Richard J. Rodenburg performed and analyzed WES, did routine metabolic tests on the patient cell line and generated the complemented patient and control cell lines. Martijn A. Huynen and Johannes N. Spelbrink conceived and designed the study of the patient cell line. Selma L. van Esveld wrote the first draft of the manuscript. All authors contributed to the data collection and analysis, manuscript revision, read and approved the submitted version.

ETHICS STATEMENT
All procedures followed were in accordance with the ethical standards of the responsible committee on human experimentation (institutional and national) and with the Helsinki Declaration of 1975, as revised in 2000. Informed consent was obtained from all patients for being included in the study.

DATA AVAILABILITY STATEMENT
The datasets generated during and/or analyzed during the current study are available in the source file or from the corresponding author on reasonable request.

ORCID
Johannes N. Spelbrink https://orcid.org/0000-0002-9756-2602

REFERENCES
1. Ojala D, Montoya J, Attardi G. tRNA punctuation model of RNA processing in human mitochondria. *Nature.* 1981;290:470-474.
2. Aloni Y, Attardi G. Symmetrical in vivo transcription of mitochondrial DNA in HeLa cells. *Proc Natl Acad Sci U S A.* 1971;68:1757-1761.
3. Murphy WI, Attardi B, Tu C, Attardi G. Evidence for complete symmetrical transcription in vivo of mitochondrial DNA in HeLa cells. *J Mol Biol.* 1975;99:809-814.
4. Borowski LS, Dziembowski A, Hejnowicz MS, Stepien PP, Szczesny RJ. Human mitochondrial RNA decay mediated by PNPase-hSuv3 complex takes place in distinct foci. *Nucleic Acids Res.* 2013;41:1223-1240.
5. Chujo T, Ohira T, Sakaguchi Y, et al. LRPPRC/SLIRP suppresses PNPase-mediated mRNA decay and promotes poly-adenylation in human mitochondria. *Nucleic Acids Res.* 2012;40:8033-8047.
6. Tu YT, Barrientos A. The human mitochondrial DEAD-box protein DDX28 resides in RNA granules and functions in Mitoribosome assembly. *Cell Rep.* 2015;10:854-864.
7. Szczesny RJ, Borowski LS, Brzezniak LK, et al. Human mitochondrial RNA turnover caught in flagranti: involvement of hSuv3p helicase in RNA surveillance. *Nucleic Acids Res.* 2010;38:279-298.
8. Jourdain AA, Koppen M, Rodley CD, et al. A mitochondria-specific isoform of FASTK is present in mitochondrial RNA granules and regulates gene expression and function. *Cell Rep.* 2015;10:1110-1121.
9. Song J, Perreault JP, Topisirovic I, Richard S. RNA G-quadruplexes and their potential regulatory roles in translation. *Translation.* 2016;4:e1244031. doi:10.1080/21690731.2016.1244031
10. Pietras Z, Wojcik MA, Borowski LS, et al. Dedicated surveillance mechanism controls G-quadruplex forming non-coding RNAs in human mitochondria. *Nat Commun.* 2018;9:2558.
11. Szczesny RJ, Borowski LS, Malecki M, Wojcik MA, Stepien PP, Golik P. RNA degradation in yeast and human mitochondria. *Biochim Biophys Acta.* 2012;1819:1027-1034.
12. Shu Z, Vijayakumar S, Chen CF, Chen PL, Lee WH. Purified human SUV3p exhibits multiple-substrate unwinding activity upon conformational change. *Biochemistry.* 2004;43:4781-4790.
13. Minczuk M, Piwowarski J, Papworth MA, et al. Localisation of the human hSuv3p helicase in the mitochondrial matrix and its preferential unwinding of dsDNA. *Nucleic Acids Res.* 2002;30:5074-5086.
14. Wang DD, Shu Z, Lieser SA, Chen PL, Lee WH. Human mitochondrial SUV3 and polynucleotide phosphorylase form a 330-kDa heteropentamer to cooperatively degrade double-stranded RNA with a 3′-to-5′ directionality. *J Biol Chem.* 2009;284:20812-20821.
15. Veno ST, Kulikowicz T, Pestana C, Stepien PP, Stevnsner T, Bohr VA. The human Suv3 helicase interacts with replication protein A and flap endonuclease 1 in the nucleus. *Biochem J.* 2011;440:293-300.
16. Szczesny RJ, Obriot H, Paczkowska A, et al. Down-regulation of human RNA/DNA helicase SUV3 induces apoptosis by a caspase- and AIF-dependent pathway. *Biol Cell.* 2007;99:323-332.
17. Silva S, Camino LP, Aguilera A. Human mitochondrial degradosome prevents harmful mitochondrial R loops and mitochondrial genome instability. *Proc Natl Acad Sci U S A.* 2018;115(43):11024-11029.
18. Jandeaux C, Kuchcinski G, Ternynck C, et al. Biometry of the cerebellar vermis and brain stem in children: MR imaging reference data from measurements in 718 children. *Am J Nueroradiol.* 2019;40:1835-1841.
19. Finn RD, Coggill P, Eberhardt RY, et al. The Pfam protein families database: towards a more sustainable future. *Nucleic Acids Res.* 2016;44:D279-D285.
20. Potter SC, Luciani A, Eddy SR, Park Y, Lopez R, Finn RD. HMMER web server: 2018 update. *Nucleic Acids Res.* 2018;46:W200-W204.

21. Wheeler TJ, Clements J, Finn RD. Skylign: a tool for creating informative, interactive logos representing sequence alignments and profile hidden Markov models. *BMC Bioinf.* 2014; 15:7.

22. Drozdetskiy A, Cole C, Procter J, Barton GJ. JPred4: a protein secondary structure prediction server. *Nucleic Acids Res.* 2015; 43:W389-W394.

23. Wang S, Peng J, Ma J, Xu J. Protein secondary structure prediction using deep convolutional neural fields. *Sci Rep.* 2016;6: 18962.

24. Meszaros B, Erdos G, Dosztanyi Z. IUPred2A: context-dependent prediction of protein disorder as a function of redox state and protein binding. *Nucleic Acids Res.* 2018;46:W329-W337.

25. Brameier M, Krings A, MacCallum RM. NucPred—predicting nuclear localization of proteins. *Bioinformatics.* 2007;23:1159-1160.

26. Kosugi S, Hasebe M, Tomita M, Yanagawa H. Systematic identification of cell cycle-dependent yeast nucleocytoplasmic shuttling proteins by prediction of composite motifs. *Proc Natl Acad Sci U S A.* 2009;106:10171-10176.

27. Minczuk M, Mroczek S, Pawlak SD, Stepien PP. Human ATP-dependent RNA/DNA helicase hSuv3p interacts with the cofactor of survivin HBXIP. *FEBS J.* 2005;272:5008-5019.

28. Castello A, Frese CK, Fischer B, et al. Identification of RNA-binding domains of RNA-binding proteins in cultured cells on a system-wide scale with RBDmap. *Nat Protoc.* 2017;12:2447-2464.

29. Chou KC, Zhang CT, Maggiora GM. Disposition of amphiphilic helices in heteropolar environments. *Proteins.* 1997;28:99-108.

30. Wadhwa R, Subramanian V, Stevens-Truss R. Visualizing alpha-helical peptides in R with helixvis. *J Open Source Softw.* 2018;3:1008.

31. Khidr L, Wu G, Davila A, Procaccio V, Wallace D, Lee WH. Role of SUV3 helicase in maintaining mitochondrial homeostasis in human cells. *J Biol Chem.* 2008;283:27064-27073.

32. Chen PL, Chen CF, Chen Y, et al. Mitochondrial genome instability resulting from SUV3 haploinsufficiency leads to tumorigenesis and shortened lifespan. *Oncogene.* 2013;32:1193-1201.

33. Hensen F, Potter A, van Esveld SL, et al. Mitochondrial RNA granules are critically dependent on mtDNA replication factors Twinkle and mtSSB. *Nucleic Acids Res.* 2019;47:3680-3698.

34. Gholijani N, Yazdani MR, Dastgheib L. Predominant role of innate pro-inflammatory cytokines in vitiligo disease. *Arch Dermatol Res.* 2020;312:123-131.

35. Dhir A, Dhir S, Borowski LS, et al. Mitochondrial double-stranded RNA triggers antiviral signalling in humans. *Nature.* 2018;560(7717):238-242.

36. Paul E, Cronan R, Weston PJ, et al. Disruption of Supv3L1 damages the skin and causes sarcopenia, loss of fat, and death. *Mamm Genome.* 2009;20:92-108.

37. Pereira M, Mason P, Szczesny RJ, et al. Interaction of human SUV3 RNA/DNA helicase with BLM helicase; loss of the SUV3 gene results in mouse embryonic lethality. *Mech Ageing Dev.* 2007;128:609-617.

38. Dmochowska A, Kalita K, Krawczyk M, et al. A human putative Suv3-like RNA helicase is conserved between Rhodobacter and all eukaryotes. *Acta Biochim Pol.* 1999;46:155-162.

39. van Esveld SL, Huynen MA. Does mitochondrial DNA evolution in metazoa drive the origin of new mitochondrial proteins? *IUBMB Life.* 2018;70:1240-1250.

40. Haen KM, Pett W, Lavrov DV. Parallel loss of nuclear-encoded mitochondrial aminoacyl-tRNA synthetases and mtDNA-encoded tRNAs in Cnidaria. *Mol Biol Evol.* 2010;27:2216-2221.

41. Duarte I, Nabuurs SB, Magno R, Huynen M. Evolution and diversification of the organellar release factor family. *Mol Biol Evol.* 2012;29:3497-3512.

42. Sharma MR, Koc EC, Datta PP, Booth TM, Spremulli LL, Agrawal RK. Structure of the mammalian mitochondrial ribosome reveals an expanded functional role for its component proteins. *Cell.* 2003;115:97-108.

43. Barreto FS, Burton RS. Evidence for compensatory evolution of ribosomal proteins in response to rapid divergence of mitochondrial rRNA. *Mol Biol Evol.* 2013;30:310-314.

44. Greber BJ, Ban N. Structure and function of the mitochondrial ribosome. *Annu Rev Biochem.* 2016;85:103-132.

45. Lavrov DV. Key transitions in animal evolution: a mitochondrial DNA perspective. *Integr Comp Biol.* 2007;47:734-743.

46. Matilainen S, Carroll CJ, Richter U, et al. Defective mitochondrial RNA processing due to PNPT1 variants causes Leigh syndrome. *Hum Mol Genet.* 2017;26:3352-3361.

47. Neveling K, Feenstra I, Gilissen C, et al. A post-hoc comparison of the utility of sanger sequencing and exome sequencing for the diagnosis of heterogeneous diseases. *Hum Mutat.* 2013;34: 1721-1726.

48. Wortmann SB, Koolen DA, Smeitink JA, van den Heuvel L, Rodenburg RJ. Whole exome sequencing of suspected mitochondrial patients in clinical practice. *J Inherit Metab Dis.* 2015;38:437-443.

49. R Core Team. *Language and Environment for Statistical Computing.* Vienna, Austria: R Foundation for Statistical Computing; 2015.

50. Warnes GR, Bolker B, Bonebakker L, et al. Gplots: various R programming tools for plotting data; 2016.

51. Wickham H. *ggplot2: Elegant Graphics for Data Analysis.* New York, NY: Springer-Verlag; 2016.

52. Wickham H. Scales: scale functions for visualization; 2017.

53. Wickham H. Reshaping data with the reshape package. *J Stat Softw.* 2007;21:1-20.